Ribosomal Crystallography and Heteropolytungstates

DANIELA JANELL*, ANTE TOCILJ*, INGO KÖLLN*, FRANK SCHLÜNZEN*, MARCO GLÜHMANN*, HARLY A.S. HANSEN*, JÖRG HARMS*, ANAT BASHAN°, ILANA AGMON°, HEIKE BARTELS*°, MAGGIE KESSLER°, SHULAMITH WEINSTEIN°, FRANCOIS FRANCESHI^, ADA YONATH*°

**MPG for Ribosomal Struct, Notkestr. 85, 22603 Hamburg, Germany*

° Dept. Struct. Biol. Weizmann Inst., 76100 Rehovot, Israel

^ MPI for Mol. Genetics, Ihnestr. 73, 14195 Berlin, Germany

Send correspondence to
A. Yonath, Weizmann Institute, Rehovot 76100, Israel
TeI:972-8-9343028, Fax:972-8-9344154,
e-mail: yonath@mpgars.desy.de

Abstract. Heteropolytungstates play a dual role in ribosomal crystallography. Beside generating phases, one of them, $(NH_4)_6(P_2W_{18}O_{62})14H_2O$, was found to be extremely useful in inducing post crystallization rearrangements. These led to a significant increase in the internal order of crystals of the small ribosomal subunits from *Thermus thermophilus,* manifested in a dramatic extension of the resolution of their diffraction patterns, from the initial 7-9 Å to 3 Å. The current 3.3 Å electron density map of this particle, constructed using phases obtained from this W cluster together with other metal compounds, shows the recognizable overall morphology of the small ribosomal subunit. Over 96% of the nucleotides were traced and the fold of all proteins was determined fully or partially. Specific sites were determined independently by covalently bound heavy atom clusters, among them the surface of two proteins and a functional center, the gate for mRNA binding. All tungsten-cluster sites detected in this map are located in close proximity to the proteins of the particle, in positions that may have an influence on the stability and the rigidity of this rather flexible ribosomal subunit.

M.T. Pope and A. Müller (eds.), Polyoxometalate Chemistry, 391–415.

1. Introduction

Ribosomes are the universal intracellular molecular machines that are responsible for one of the most fundamental life processes, the translation of the genetic code into proteins. They are giant nucleoprotein organelles built of two independent subunits of unequal size which associate upon the initiation of protein biosynthesis. In bacteria their molecular weight is about 2.3 mega dalton and they are comprised of RNA and proteins at a 2:1 ratio. The small subunit (called 30S for eukaryotic ribosomes, according to its sedimentation coefficient), is of molecular weight of 0.85 mega dalton and consists of 20-21 proteins and one RNA chain of about 1500 nucleotides (called 16S RNA). It offers the site for the initiation and the progression of the biosynthetic process and facilitates the decoding of the genetic information. The large subunit (50S) catalyzes the formation of the peptide bond and provides the path for the progression of the nascent proteins. It is of molecular weight of about 1.45 mega dalton and contains two RNA chains (called 23S and 5S RNA) of a total of about 3000 nucleotides and 36-50 different proteins, depending on the source.

Crystals have been obtained from several ribosomal particles, diffracting best to around 3 Å, among them the small and the large ribosomal subunits from *T. thermophilus,* called T30S and T50S (Yonath et al., 1998; Bashan et al., 2000) and of the large ribosomal subunit from *Haloarcula marismortui*, H50S (von Böhlen et al., 1991). However, the bright synchrotron radiation that is essential for resolving the higher resolution terms, namely at the 3-5 Å shell, causes rapid radiation damage within a period sufficient for the collection of only small fractions of the data (about 1-3° of oscillation). Coupled with low level of isomorphism and/or space group variability (Makowski et al., 1987; Yonath et al., 1998; Ban et al., 1999), this extreme radiation sensitivity introduces substantial difficulties in the construction of complete data sets, mainly because the low level of isomorphism of the ribosomal crystals. To minimize the number of crystals needed for producing complete sets, they are irradiated by a beam with a cross-section smaller than their size. Once decay is observed, the crystals are being translated, and a new area is being irradiated. This approach was the key for crossing the 5 Å border in data collection, and for obtaining high quality data sets from the rod-like crystals of T30S, that may reach the dimensions of **500x60x60** microns.

The assignment of phases to the observed structure factor amplitude is the most crucial, albeit most complicated step in structure determination. Since the phases cannot be directly measured, their elucidation remains the least predictable task, even for average-size proteins. Multiple and single isomorphous replacement (MIR and SIR) and multiple anomalous dispersion (MAD), are the commonly used methods for phasing diffraction data from crystals of biological macromolecules. All require the preparation of heavy

atom derivatives in which electron-dense atoms are inserted into the crystalline lattice at distinct locations. As the changes in the structure factor amplitudes resulting from the addition of the heavy atoms are being exploited, the derivatization reagents are chosen according to their potential ability to induce measurable signals. Whereas single metal atoms yield signal sufficient to phase data collected from crystals of average size proteins, owing to the large size of the ribosomal particles, dense heavy atom clusters seem to be advantageous (Thygesen et al., 1996). Heteropolytungstates were found to be extremely useful in this respect and a detailed account of these findings is given below. Additional examples are the smaller compounds, Ta_6Br_{14}, a tetra mercury compound, TAMM, and a tetra iridium cluster, TIR (Jahn, 1989). Among them, Ta_6Br_{14} yielded phase information for all ribosomal particles currently being studied, namely, T30S, T50S, T70S and H50S (Thygesen et al., 1996; Yonath et al., 1998; Clemons et al., 1999; Ban et al., 1999; Cate et al., 1999; Tocilj et al., 1999; Schlünzen et al, 2000).

The other two compounds, TIR and TAMM were designed to bind covalently to exposed sulfhydryls and led to the localization of two ribosomal proteins of the small subunit, S11 and S13 (Weinstein et al., 1999). In the studies of T30S, they also provided tools for targeting functional sites in which ribosomal RNA is involved (Weinstein et al., 1999; Auerbach et al., 2000; Bartels et al., 2000). Thus, they were bound to tailor made ligands, such as antibiotics or DNA oligomers complementary (cDNA) to exposed single strand rRNA regions, that were either co-crystallized with the T30S subunit or diffused into the already formed crystals. One of these is a 22-base DNA oligomer, complementary to the 3' end of the 16S RNA. This region, which is known to be rather flexible (Müller and Brimacombe, 1997), contains the anti Shine-Dalgarno sequence. Therefore the DNA oligomer complimentary to it was considered as the mRNA analog that participates in the formation of the initiation complex. The diffusion and hybridization of a heavily mercurated form of this oligomer into T30S led to a derivative diffracting very well to a high resolution. Therefore it is suggested that the hybridization of the 16S RNA with this oligomer limits the mobility of the flexible 3' arm of the 16S RNA, in a fashion that mimics the binding of mRNA.

2. Heteropolytungstates in Ribosomal Crystallography

The strategy proved, so far, most suitable for phasing ribosomal data is based on the determination of an initial phase set at low resolution. This may be extended later, by experimental or computational methods. Molecular replacement exploiting cryo EM reconstructions proved useful for H50S (Ban et al., 1999), T50S (Yonath and Franceschi, 1988) and for the whole ribosome from *T. thermophilus,* T70S (Cate et al., 1999; Harms et al., 1999). For T30S, however, despite extensive attempts, no solution was obtained, perhaps because of its multi-conformational nature and inherent flexibility (Gabashvili et al., 1999; Harms et al., 1999). Therefore phasing was performed by measuring data from derivatized crystals. Advantage was taken of dense compounds containing a large number of heavy-atoms, arranged in close proximity (Thygesen et al., 1996). These were used either for pre-crystallization covalent binding at preferred locations (Weinstein et al., 1999), or for traditional soaking experiments. Despite the large size of the clusters that may have hampered their penetration into the crystals, many of the soaking experiments were successful, presumably because the ribosomal crystals contain wide internal solvent channels. Furthermore, it seems that for crystals with wide solvent regions, the large size of these compounds is advantageous, as it limits their free movement and minimize multiple site binding.

Heteropolytungstates (e.g. Dawson, 1953; Pope and Papaconstantinou, 1967; D'Amour, H., 1976; Brown et al., 1977; Contant, R., 1990; Xin and Pope, 1994; Wei et al., 1997) yielded useful derivatives in crystallographic studies of several biological macromolecules, all by soaking experiments. These large anions are of exceptional stability over a wide range of pH and redox states. They posses a high degree of internal symmetry, and a correlation between it and their binding sites has been detected. In such cases they were found suitable for high resolution phasing. An example is the structure of riboflavin synthase (Ladenstein, et al., 1987) that possess an internal five fold symmetry, which coincided with that of $(NaP_5W_{30}O_{110})^{-14}$ (Alizadeh et al., 1985). However, in the absence of preferred orientation, the effective phasing resolution is limited to 4-5 Å, even when sophisticated spherical averaging techniques are being used (Fu et al., 1999). Nevertheless under favorable conditions, the W18 clusters did bind in a specific way, so that its individual W atoms could be resolved at resolution higher than 4.5 Å, and used for phasing.

In ribosomal crystallography the heteropolytungstates were found to be very suitable for phasing at low resolution, as well as for the validation of the results obtained by molecular replacement searches (Ban et al., 1999). So far, reports of materials that generated phases include: W12 $(Na_{16}[(O_3PCH_2PO_3)_4W_{12}O_{36}]40H_2O)$ and W17 $(Cs_7(P_2W_{17}O_{61}Co(NC_5H_5))14H_2O)$ (Yonath et al., 1998), as well as W9 $[(phSn)_4(AsW_9O_{33})_2]$ and $W11Rh{=}Cs_5(PW_{11}O_{39}[Rh_2CH_3COO_2]$ (Ban et al, 1999) were

used in phasing the data of the halophilic large subunit. $H_4SiO_4[12WO]$ and $Li_{10}(P_2W_{17}O_{61})$ (Clemons et al., 1999) as well as W18 $((NH_4)_6(P_2W_{18}O_{62})14H_2O)$, and W4 $((TMA)_2Na_2[Nb_2W_4O_{19}]18H_2O)$ (Tocilj et al., 1999) were used for the determination of the medium resolution structure of the thermophilic small ribosomal subunit.

2.1 THE WONDERS OF W18

Neither of the ribosomal crystal types that diffract to molecular resolution was obtained solely from purified ribosomal particles. In all cases additives had to be used, each in a different fashion. Initially, small metal compounds were screened for their influence on the crystal's properties. Among them, minute amounts of Cd^{++} in the crystallizing droplet led to significant gain in the internal order of the H50S crystals, as expressed in resolution increase from 6-7 to 2.7-3 Å. A systematic search included larger and more complex materials, as well as various modes of their addition, led to the improvement of the crystals of T30S by post crystallization treatments by minute amounts of a heteropolytungstate cluster, W18.

As subjects for crystallization, the small ribosomal subunit is less suitable than the entire ribosome or its large subunits. Cryo electron microscopy (Stark et al., 1995; Frank et al., 1995), surface RNA probing (Alexander et al., 1994) and monitoring the ribosomal activity (Weller and Hill, 1992) showed that among the ribosomal particles, the small ribosomal subunit displays the highest conformational variability. This inherent flexibility may be the reason for the low resolution (about 10 Å) of the early crystals of T30S (Yonath et al., 1988; Trakhanov, et al., 1989). It also may account for the unsuitability of all the available cryo-EM reconstructions of the small ribosomal subunit for extracting initial phase sets, studies that, as mentioned above, were performed successfully for the large ribosomal subunit, H50S and T50S (Ban et al., 1999; Harms et al., 1999).

The dramatic improvement in crystal quality was not accompanied by changes in the unit cell dimensions or in the crystal symmetry (a=b=407 Å, c=176 Å, $P4_12_12$). However, data collected from the W18 treated crystals (called here Wative) could not be scaled to the data obtained from the original native crystals, indicating significant non-isomorphism and suggesting that a major conformational rearrangement occurred upon the W18 treatment. Among the many tungsten compounds tested by us (most of the material listed in TABLE I), so far only W18 was found suitable for the increase in resolution. Furthermore, soaking washed Wative crystals (called here back-soaked or BS crystals) in solutions containing $W9_2$, a compound closely related to W18, led to diffraction that could not be scaled with that obtained from Wative or BS crystals, most likely due to additional post-crystallization conformational rearrangements.

Interestingly, in studies performed independently on T30S crystals that were grown under the same conditions (Yonath et al., 1988), a related compound, $Li_{10}(P_2W_{17}O_{61})$, was used for phasing. This compound, however, was found to reduce, rather than to increase, the resolution (Clemons et al., 1999).

Conformational changes are not routinely induced within crystals due to the limitation of the motion imposed by the crystal network. However, realizing that the T30S crystals tolerate and even benefit from internal rearrangements, prompted us to induce reactivation of the T30S particles within the crystals. Controlled heating, the common procedure for functional activation of ribosomal particles (Zamir et al., 1971), was employed on entire crystals, enabling quantitative binding of compounds participating in protein biosynthesis or their analogs (Auerbach et al., 2000; Bashan et al., 2000).

It is conceivable that other metals could have led to a similar effect on ribosomal crystals. Thus, hints for the improvement of crystal order by Os hexamine chloride may be extracted from the facts that derivatization with this compound leads to non-isomorphous crystals that diffract to higher resolution (Clemons et al., 1999). This compound has already been used for improving RNA crystals (Cate and Doubna, 1996; Golden et al., 1998). It is known to interact with RNA chains in a specific fashion that may increase their rigidity. Hence, it is conceivable that the improvement of the internal order of the T30S subunits by this compound is linked to its binding property.

TABLE 1: TUNGSTEN COMPOUNDS USED IN THIS STUDY

Sodium tungstate

WAC = $W_3O_2(acetate)_6(H_2O)_3CF_3SO_3$

W4 = $(TMA)_2Na_2[Nb_2W_4O_{19}]18H_2O$ +

W11SiRh = $Cs_5H_xSiW_{11}O_{39}Rh^{III}CH_3COO(H)$ *

W12(Na) = $Na_{16}[(O_3PCH_2PO_3)_4W_{12}O_{36}]40H_2O$

W12(K) = $K_5H(PW_{12}O_{40})12H_2O$ +

PhSnW15 = $K_5H_4[(phSn)_3(P_2W_{15}O_{59})]16H_2O$

BuSnW15 = $K_5H_4((buSn)_3(P_2W_{15}O_{59})]15H_2O$

W17CsCo = $Cs_7(P_2W_{17}O_{61}Co(NC_5H_5))14H_2O$ +

W17LiCo = $Li_7(P_2W_{17}O_{61}Co(NC_5H_5))14H_2O$

BuSnW17 = $K_7[(buSn)(P_2W_{17}O_{61})]10H_2O$

W17-Th = $Cs_7(P_2W_{17}O_{61}Th(NC_5H_5))nH_2O$ *

$W9_2$ = $K_4H_3[(buSn)_3(a\text{-}SiW_9O_{31})_2]nH_2O$

W18 = $(NH_4)_6(P_2W_{18}O_{62})14H_2O$ +

W30 = $K_{14}(NaP_5W_{30}O_{110})31H_2O$

bu=butyl; ph=phenyl

TMA=tetra methyl ammonium

* Designed for covalent binding

+ Found useful for phasing or for map interpretation

2.2. DOUBLE-DERIVATIVE PHASING

2.2.1. Strategies in derivatization: A Flexible Definition of Native Crystals

The chemical basis for the increase in the order of the T30S crystals by W18 is still far from being fully understood. Nevertheless, careful studies led to several interesting observations. It was shown by inductively coupled plasma mass-spectrometry and atomic emission spectrometry, that although minute quantities of W18 are needed for successful treatment, relatively large amount of this cluster penetrate into the crystals and resides within them. These quantities are much higher than those detected by crystallographic methods, meaning that some W18 clusters are flowing in the solvent regions.

As the original T30S native crystals became obsolete by the W18 treatment, a new definition for native crystals had to be made. Initially, the Wative crystals were considered as native. These were further derivatized by soaking in solutions containing additional heavy atom derivatives (TABLE II). However, it was found that the flouting W18 clusters complicated the phasing process, since the non-bound W18 clusters led to high background, which, in turn, "masked" the contribution of the additional heavy atoms. Furthermore, these solubilized clusters generated measurable anomalous signals at low resolution which could not be separated from those originating from the specifically bound ones. Since the major phasing contribution of W18 is in the medium and the low resolution shells, a large fraction of the phasing information was lost, or led to confusion.

A more defined crystal-system was obtained by washing the Wative crystals. As the washed crystals diffract to resolution comparable to that obtained from the Watives, it was assumed that the main W18 sites that are contributing to the improvement of the crystal order are occupied even after the wash. This assumption was later verified by crystallographic anomalous measurements of the back-soaked crystals, as well as by the examination of the content of dissolved washed crystals (see below, in chapter 3.2). Indeed, it was found by the methods described above, that a large amount of W18 remains within the crystals even after applying an extensive washing procedure (twelve times during 40-50 hours).

Knowing that the Wative as well as the BS crystals contain significant amounts of W18, the choice, the combination and the design of the heavy atom derivatization was dictated not only by their potential ability to produce phases, but also according to the chemical properties of the combined systems. Consequently, the further derivatization steps were performed by soaking the Wative crystals in heavy atom solutions, in the presence or in the absence of W18, as dictated by the stability of the crystals.

Table II: Double Derivative Phasing Statistics.

Derivative	Unique Refl.	Resol. (Å)	Complete-ness (%)	R_{sym} (%)	R_{merge} (%)	Phasing power	R_{cullis}	Sites
	a) „Natives“							
BS (Native)	122788	3.8 (•)	86.4	12.7	-	-	-	-
Wative 1	206724	3.3	94.7	13.6	17.9	1.2	0.74	4
Wative 2	133199	3.5	80.5	10.6	16.6	1.5	0.77	3
Wative (ano)	42995	7.0	99.1	7.6	17.2	1.6/1.1 (†)	0.4/0.8 (†)	3
	b) Double soaks							
Ta_6Br_{14}	48132	5.0	56.1	14.3	26.6	1.4	0.84	3
$Hg_3C_6O_4H_8$ (‡)	17092	6.5	60.1	14.4	22.9	1.3	0.73	7
$C_2Hg_6N_2O_8$	55800	5.9	79.6	6.9	21.7	1.7	0.50	4
PIP (§)	62015	4.5	80.9	14.1	17.5	0.5	0.91	6
K_2O_4Os	49751	5.0	77.9	14.7	22.9	1.0	0.68	7
Pb_3-citrate (‡) (¶)	26982	6.4	92.4	11.1	14.6	1.1	0.79	8
$NaAuCl_4$	30078	5.5	81.0	13.6	15.5	1.0	0.78	1
W_4 (§)	26748	6.4	91.8	11.8	15.0	0.9	0.72	4
K_2PtCl_4 (‡)	23551	6.5	81.5)	11.1	20.9	0.8	0.90	7
AquaPt (§)	28439	5.0	49.3	15.9	26.1	0.6	0.85	5
CisPt (§)	19366	6.9	80.7	9.9	18.1	0.6	0.84	3
	c) Covalent binding							
OliT (‡) (¶) (§)	36083	4.8 (‖)	58.1	14.2	14.9	3.1	0.71	1
TAMM (§)	25797	7.0	60.3	10.7	16.4	0.6	0.94	2
TIR (‡) (§) (¶)	43424	4.5	57.3	8.5	21.4	0.6	0.88	2
M-HgAc (‡) (¶)	29719	6.0	80.6	13.7	16.2	1.2	0.66	6
U-Ac (‡) (¶)	30911	6.0	84.4	12.3	15.3	0.5	0.85	5

$R_{sym} = \Sigma | I - \langle I \rangle | / \Sigma \langle I \rangle$, $R_{merge} = \Sigma | F_{PH} - F_P | / \Sigma F_P$, $R_{cullis} =$ <phase-integrated lack of closure>/ $< | F_{PH} - F_P | >$, Phasing power = $< [| F_H (calc) | /$ phase-integrated lack of closure] >.
(•) Data were collected to 3Å, but not used in this study, (†) iso/ano, (‡) SIR, not incorporated yet, (§) See abbreviation, (¶) Wative was considered as native, (‖) Data were collected to 3.5Å, but not used in this study.

In a few cases the addition of the heavy atom cause crystal deterioration unless some of the internal W18 was removed before further soaking. The treatment was also applied to crystals containing analogs of compounds participating in protein biosynthesis as well as to those that were specifically modified by covalent binding.

2.2.2. Phasing at Narrow and Wide Resolution Ranges

Two approaches were taken for phasing the data obtained from the W18 treated derivatives T30S crystals. The "narrow range" strategy, employed only at the initial stages of these studies, was based on minimizing the contribution of the W18 to the diffraction patterns, regarding it as part of the crystal solvent. The borders of this range were determined according to two factors: the highest resolution of the derivatives and the range that was supposed to be effected by the presence of the W18, namely lower than 10-12 Å. Since at the initial stages of this study the heavy atom derivatized crystals diffracted to around 7 Å, the useable resolution shell for the narrow range phasing was between 7 to 12 Å.

The narrow range phasing procedure was found to be lengthy and demanding since in order to produce measurable signals from crystals of very large macromolecules which cannot be subdivided by non-crystallographic symmetry, multiple site derivatization is required. The identification and the refinement of these sites was found to be rather demanding, especially due to the requirement for careful cross-verifications (Schlünzen et al., 1999; Weinstein et al., 1999). Over fifty sites originating from four heavy atom derivatives were extracted from overcrowded and rather flat difference Patterson maps. These studies led to a 7.2 Å MIR map that could be partially interpreted, but suffered from considerable fragmentation (Schlünzen et al., 1999; Weinstein et al., 1999; Bashan et al., 2000).

The parallel approach, based on the incorporation of all available phase information was proved to be more suitable, despite the experimental and conceptual complications originating from the presence of unknown amount of W18 in the crystals. Owing to the non-isomorphism between the native and the Wative data, the sites of W18 in the Wative crystals could not be revealed by difference Patterson techniques. However, four sites with exceptionally high signals were identified in difference Patterson combined with cross Fourier maps, constructed from Wative and BS diffraction data (Figure 1).

W18, by itself, contributed significantly to the progress of the phasing process. As mentioned above, the resolution of the back-soaked crystals is as high as that of the Watives. Therefore it was assumed that the sites of W18 that cause the increase in resolution are occupied in the BS crystals despite the extensive washing steps.

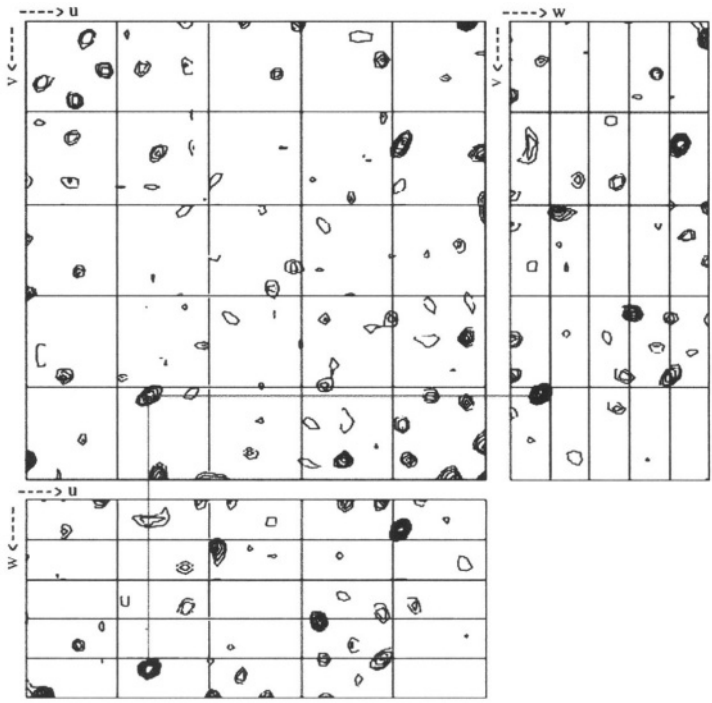

FIGURE 1: Three Harker sections of the difference Patterson map, using data collected from Wative and back soaked (BS) crystals, constructed at 9 Å resolution and showing the main W18 site.

Fluorescence spectra measured from the BS crystals indicated the presence of W18 in these crystals (Figure 2). Anomalous signals, originating from W18, were readily resolved by collecting data at two wavelengths, reconfirmed the above assumption. These data also cleared the space group ambiguities between the two enantiomers, $P4_12_12$ and $P4_32_12$ and their incorporation in a previous 7 Å map led to an increased level of detail (Figure 3).

The sites of the additional heavy atoms (TABLE II) were determined and verified by difference Patterson and cross Fourier procedures. The initial wide-range map was calculated at the 7-30 Å resolution shell, using phase information from W18 and Ta_6Br_{14}. The latter was instrumental in bridging between the lower resolution information, obtained from W18, and the higher resolution phases that were extracted from the data obtained from smaller heavy atom derivatives.

The exceptionally strong phasing power of the W18 cluster biased frequently the difference Patterson maps of the additional derivatives. Nevertheless, by careful interplay, most of the sites of the additional derivatives were revealed and reconfirmed. These enabled the computation of a 3.3 Å MIRAS map, phased exclusively by crystallographic methods, with no need for the incorporation of electron microscopy or otherwise constructed models. In these studies the clusters were first treated as group scatterers or a spherical averaged compounds. As such, they yielded phase information to about 7 Å. Later on we took advantage of those W18 clusters that were specifically bound and used them at close to atomic resolution.

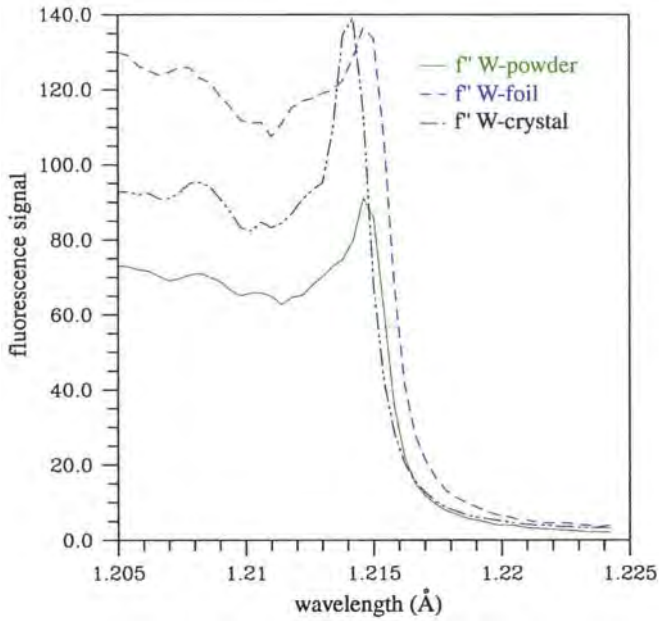

FIGURE 2: f'' as a function of wavelength, as derived from fluorescence spectra measured from a W foil, W powder and a crystal soaked in a W18 solution, all measured around the W L_{III} edge.

FIGURE 3: Part of the RNA chain together with one of the regions that became interpretable by the incorporation of the BS anomalous data at 7 Å (shown as rendered map in white). The circled insert focuses on a detail taken from a similar area (not shown here), exhibiting the typical features of helix-bulge-helix motif. Anomalous data were collected at the L_{III} edge of W (1.218 and 1.2734 Å). Experimental procedures are described in (Tocilj et al., 1999). All fitted models shown in this manuscript, were obtained interactively, with the program O (JONES et al., 1991).

3. The 3.3 Å electron density map

3.1. FEATURES SEEN IN THE SMALL RIBOSOMAL SUBUNIT AT 3.3 Å

The overall structure of the small ribosomal subunit, as seen in the 3.3 Å MIRAS map calculated with the wide-range phases (Schlünzen et al., 2000), is remarkably similar to most of the electron microscopical reconstructions of this particle at its functionally active conformation. It contains many of the recognizable features, including the traditional division into three main parts: a rather large head, a short neck and a bulky lower body (Stark et al., 1995; Frank et al., 1995; Gabashvili et al., 1999) (Figure 4 LEFT).

This map showed clearly the backbone of the RNA and in many regions bases were well separated and purines and pyrimidines could be assigned. Likewise, many of the proteins loop and side chains could be identified (Figure 4 RIGHT). The RNA chain was traced directly from the map and later compared with the available diagrams of the RNA secondary structure. Localization of the proteins was based on the large body of non-crystallographic information, as described in (Tocilj et al., 1999). Consequently this 3.3 Å map contains over 1450 (96%) of the nucleotides and the main fold of all 19 ribosomal proteins belonging to this subunit. It shows known as well as newly detected folding and packing motifs. It provides insight into the decoding mechanism and its universality, and highlights the role of selected components in maintaining the sophisticated architecture of the ribosome (Schlünzen et al., 2000).

Three long helices run parallel to the long axis of the subunit. Among them, two are located on the rather flat surface that faces the 50S subunit. These extended RNA helical elements transmit structural changes, correlating events at the particle's far end with the cycle of mRNA translocation at the decoding region, which is located about 150 Å away, at the connection between the body and the head. The three longitudinal helices are linked by transverse features, placed like ladder rungs between them. The head contains mainly short helices, in marked contrast to the long duplexes of the body. It has a bi-lobal architecture, with one helix serving as the bridge between the two hemispheres. The head joins the body through a single RNA helix which appears to act as a hinge.

The decoding center, which organizes mRNA and tRNA translocation and controls the fidelity in codon-anticodon interactions, is located at the upper part of the body and the lower part of the head. Its most prominent feature is the portion of the helix that forms most of the intersubunit contacts in the assembled ribosome H44 (also called the "penultimate stem"), which bends towards the neck. The channel through which the

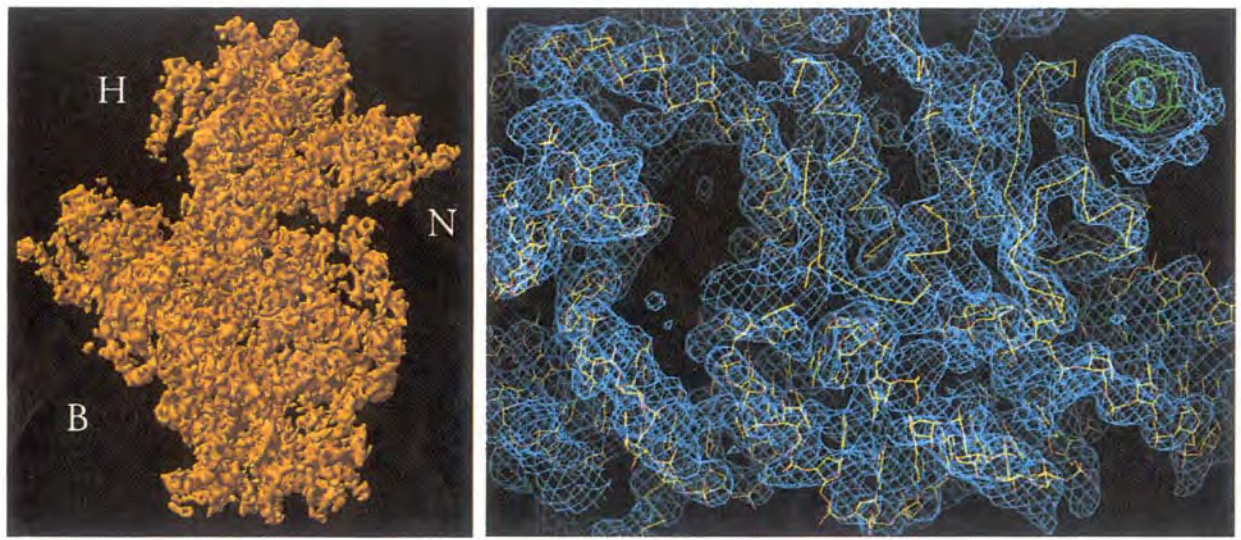

FIGURE 4: LEFT: The overall structure of the small ribosomal subunit, as extracted from the 3.3 Å map, with the traditional division into the three main parts: head (H), neck (N) and body (B). RIGHT: A region of the originally calculated 3.8 Å map showing RNA segments, the ribosomal Protein S8 and a tungsten cluster (green sphere).

messenger RNA (mRNA) progresses is located between the upper part of the body and the lower part of the head. The entrance to it can encircle the message when a latch-like contact, formed by the upper part of the body's shoulder and the lower part of the nose, closes.

All the major functional features of the subunit consist of RNA elements; the proteins appear to serve largely as struts, linkers and supports. Of interest are long extensions of proteins which penetrate into rRNA regions. Some of them reach distal proteins. Only one protein is located at the RNA-rich surface that interacts with the large subunit. Two additional proteins are located at the rims of the subunit interface region, and may be partially involved in tRNA binding or in inter subunit contacts, respectively. A few proteins may contribute to the fidelity and the directionality of the translocation. About half a dozen are peripheral, located on the particle's surface, at its solvent side. These were the hooks for W18 binding.

The smaller heavy atom markers led to independent positioning of two ribosomal proteins that possess exposed sulfhydryls, namely S11 and S13. It also revealed the location of the 3' end of the 16S RNA, highlighting the environment of the gate for mRNA binding, namely the Shine-Dalgarno sequence (Weinstein et al., 1999; Auerbach et al., 2000; Tocilj et al., 1999). The location of one of the two proteins, S13, found this way is in agreement with those suggested by neutron scattering (Moore et al., 1985), immunoelectron microscopy (Stöffler and Stöffler-Meilicke, 1986) and modelling based on crosslinking and enzymatic data (Müller and Brimacombe, 1997). For protein S11 the situation is somewhat different. Its position in the electron density map is in accord with those proposed by electron microscopy and by modeling, but differs from that obtained by neutron scattering, by a distance larger than the expected diameter of this protein.

3.2 DOES W18 STABILIZE FLEXIBLE REGIONS WITHIN THE SMALL RIBOSOMAL SUBUNIT?

The ability of W18 to induce controlled conformational rearrangements, in a fashion that increases dramatically the internal order within crystals of a cellular organelle as large as the small ribosomal subunit, is a remarkable property. Although still far from being fully understood, as shown in this study, the advantage gained by the exploitation of this property for the crystallographic studies of T30S is evident.

The strongest bound W18 molecules are those revealed in the BS crystals. It is conceivable that these are the sites that trigger the conformational changes that lead to the dramatic increase in resolution. All seven W18 sites that were detected, even after intensive back-soak, are located in close proximity to proteins, in positions which may

significantly reduce the mobility of the entire T30S particles within the crystal network. Pairing of T30S particles around the crystallographic two fold axis is one of the main features of the map of T30S (Harms et al., 1999; Tocilj et al., 1999). The contacts holding the pairs together are extremely stable, so that they are maintained even after the rest of the crystal network is destroyed. Large proportions of butterfly-shaped pairs have been observed by electron microscopy in samples of thoroughly washed and dissolved T30S crystals (Figure 5). It was found that these pairing contacts are formed by the W18 clusters that are clearly observed at the interface between the particles in the electron density map (Figures 6 and 7).

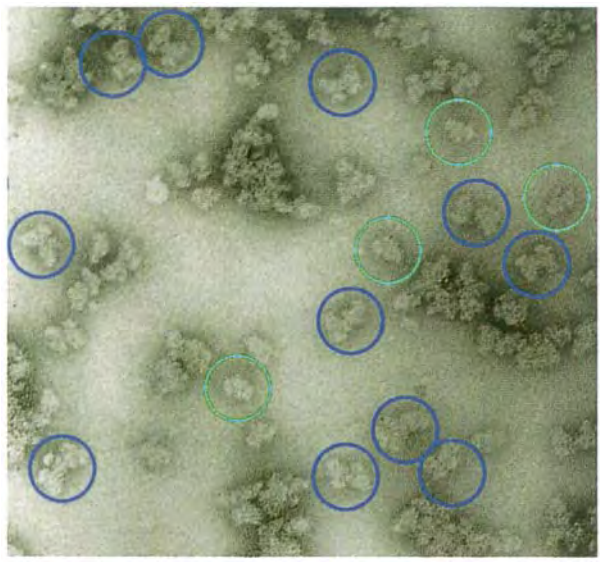

FIGURE 5: A negatively stained preparation of carefully dissolved Wative crystals as observed by transition electron microscopy, showing the butterfly-like T30S pairs (in blue circles) together with isolated particles (in cyan).

It should be noted that in the medium resolution (4.5 Å) and in the higher resolution (3.3 Å) map, all parts of the electron density of T30S seems to be equally resolved (Tocilj et al., 1999; Schlünzen et al., 2000). However, in the independently determined structure of T30S (Clemons et al., 1999) at 5.5 Å, a fair part of the "head" appears to be less well resolved. The higher clarity of our maps can not be simply connected to the higher resolution of our studies, since apart from the head, the overall shapes of our 4.5 Å and their 5.5 Å maps are in fairly good agreement. It is likely, however, that the gain in the internal order in this flexible feature is due to the W18 stabilization of the post-crystallization functionally activated particles.

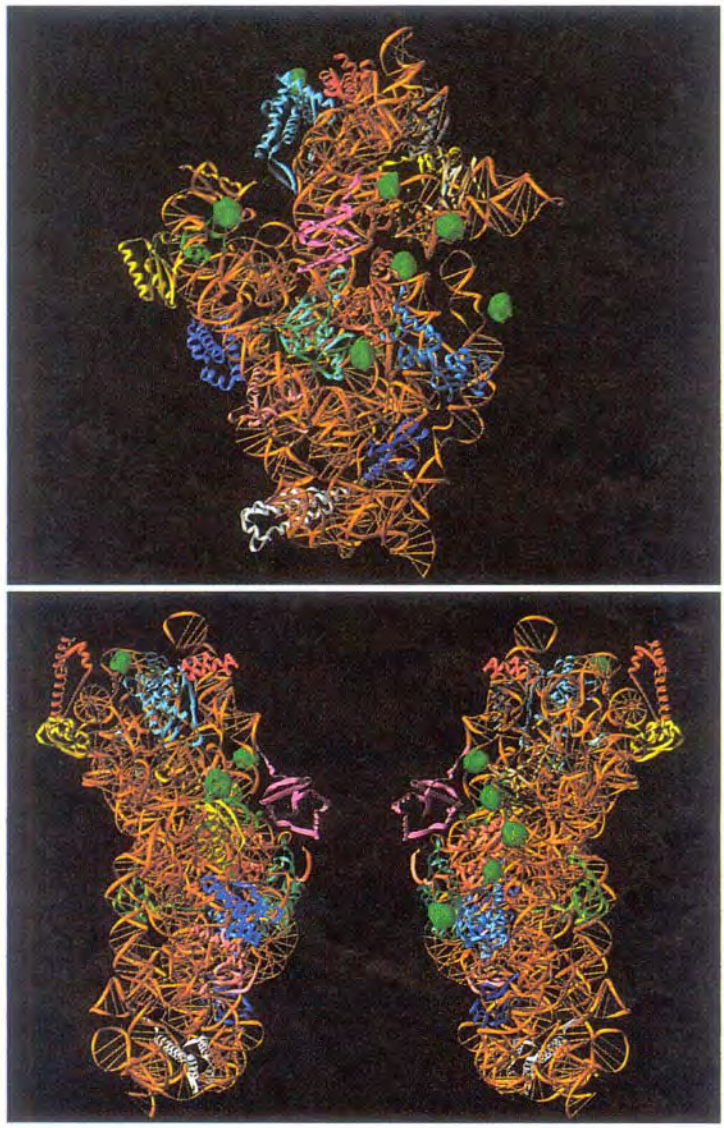

FIGURE 6: TOP: The complete model of T30S with the 16S RNA in orange and all fully or partially determined proteins in different colors. The positions of the W18 clusters are shown as green balls. BOTTOM: Two small ribosomal subunits placed in butterfly-like pairs. It is clearly seen that most of the positions of W18 clusters are on the contact side.

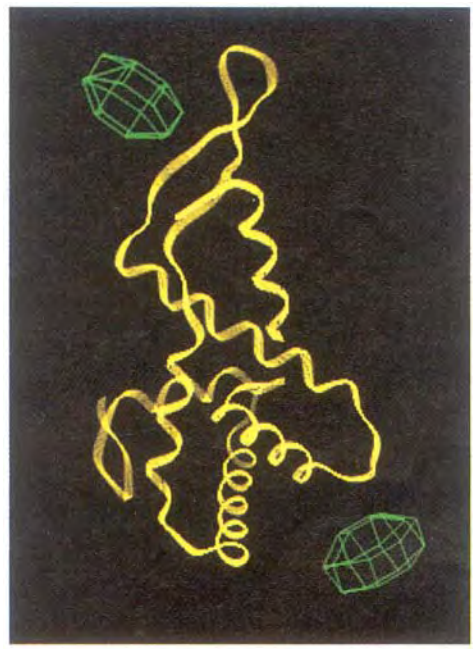

FIGURE 7: The position of two W18 clusters in close proximity to protein S7 (shown without residues 1-13).

The tendency of the heteropolytungstates to bind to relatively narrow solvent paths was detected not only at the tight interface area between the two particles consisting the T30S pairs, but also in internal cavities of other ribosomal crystals. One of these is the main tunnel of the large ribosomal subunit (Yonath et al., 1987). This tunnel is believed to provide the path used by nascent protein chains, once they are synthesized. Its approximate length, about 100 Å, and its diameter, up to 25 Å, were determined by three dimensional image reconstruction using diffraction data obtained from two dimensional sheets (Yonath et al., 1987). It took almost a decade until the existence of the this tunnel was reconfirmed by cryo electron microscopy (Stark et al., 1995; Frank et al., 1995) as well as by X-ray crystallographic studies (Yonath and Franceschi, 1998). However, the chemical nature of the walls of this tunnel and the mechanism that allows the movement of nascent proteins are still not known, although results of preliminary experiments suggested that part of these walls are built of RNA (Gewitz et al., 1988). Indications for the attachment of heteropolytungsten clusters (W30, W18 and W12) to the inner walls of this tunnel in H50S ribosomal subunits have been obtained at 7-8 Å resolution in our laboratory (data not shown), as well as at higher resolution. Thus, at 5 Å, four W11Rh molecules were detected within this tunnel (Ban et al., 1999).

4. Conclusions

We have shown that treatment of ribosomal crystals with a heteropolytungstate introduces significant internal order that lead to a striking increase in their resolution. Although the mechanism of this process has not been revealed yet, there are indications that the W18 cluster interacts with the ribosomal particle in a fashion that may reduces its internal mobility. Most of the interactions of W18 identified so far are made with ribosomal proteins. Despite the experimental complications generated by the W18 treatment, these heteropolytungstates were found to be suitable for crystallographic studies of very complex and sensitive biological macromolecules at high resolution.

Abbreviations: 70S, 50S, 30S: the whole ribosome and its two subunits from prokaryotes. A letter as a prefix to the ribosomal particles or ribosomal proteins represent the bacterial source (T=*Thermus thermophilus*; H=*Haloarcula marismortui*). tRNA and rRNA: transfer and ribosomal RNA. Small subunit proteins are named S and a running number, according to their sequence homology to *E. coli*; BS: back-soaked crystals; Wative: W18 treated crystals; SIR & MIR: single and multiple isomorphous replacement; SR: synchrotron radiation; TAMM: tetrakis(acetoxymercuri)-methane; TIR: a tetrairidium cluster; aquaPt: cis-di-aquacisplatin; cisPt: cis-$[Pt(NH_3)_4)]$; PIP: di-iododiplatinum (II) diethyleneamine; Hg_6: $C_2Hg_6N_2O_8$; Hg_3: $Hg_3C_6O_4H_8$; OliT: the TAMM modified DNA oligomer that compliments the 3'end of the 16S RNA

ACKNOWLEDGEMENTS

We thank M. Pope, W. Preetz and W. Jahn for their generous gifts of heavy atom compounds, M. Wilchek for indispensable advice, M. Safro and I. Levin for active participation, W. Traub for fruitful discussions, and R. Albrecht, T. Auerbach, H. Avila, W.S. Bennett, H. Burmeister, C. Glotz, Y. Halfon, K. Knaack, M. Laschever, S. Meier, J. Müssig, M. Pioletti, M. Peretz, C. Radzwill, M. Simitsopoulou and R. Zarivach for contributing to different stages of these studies, and to the synchrotron radiation facilities staff: EMBL & MPG beam lines at DESY; F1/CHESS; ID2 and ID14 at ESRF; ID19/APS at Argonne Nat. Lab. Support was provided by the Max-Planck Society, the US National Institute of Health (NIH GM 34360), the German Ministry for Science and Technology (BMBF 05-641EA) and the Kimmelman Center for Macromolecular Assembly at the Weizmann Institute. AY holds the Martin S. Kimmel Professorial Chair.

REFERENCES

Alexander, R. W., Muralikrishna, P. and Cooperman, B.S. (1994). Ribosomal components neighboring the conserved 518-533 loop of 16S rRNA in 30S subunits. *Biochemistry* **33**, 12109-12118.

Alizadeh, M.H., Harmalker, S.P., Jeannin, Y., Martin-Frere, J. and Pope, M.T. (1985). A heteropolyanion with fivefold molecular symmetry that contains a nonlabile encapsulated sodium ion. The structure and the chemistry of $(NaP_5W_{30}O_{110})^{-14}$. *J. Am. Chem. Soc*. **107**, 2662-2669.

Auerbach, T., Pioletti, M., Avila, H., Anagnostopoulos, K., Weinstein S., Franceschi, F. and Yonath, A. (2000). Genetic and biochemical manipulation of the small ribosomal subunit from *T. thermophilus* HB8. *Biomolecular Structure and Dynamics* **17**, 617–628.

Ban, N., Nissen, P., Capel, M., Moore P. and Steitz, T. (1999). Placement of protein and RNA structures into a 5 Å resolution map of the 50S ribosomal subunit, *Nature* **400,** 841-847.

Bartels, H., Glühmann, M., Janell, D., Schlünzen, F., Tocilj, A., Bashan, A., Levin, I., Hansen, H.A.S., Harms, J., Kessler, M., Pioletti, M., Auerbach, T., Agmon, I., Avila, H., Simitsopoulou, M, Weinstein, S., Peretz, M., Bennett, W.S., Franceschi, F. and Yonath, A. (2000). Targeting exposed RNA regions in crystals of the small ribosomal subunits at medium resolution. *Cellular and Molecular Biology,* in press.

Bashan, A., Pioletti, M., Bartels, H., Janell, D., Schlünzen, F., Glühmann, M., Levin, I., Harms, J., Hansen, H.A.S., Tocilj, A., Auerbach, T., Avila, H., Simitsopoulou, M., Peretz, M., Bennett, W.S., Agmon, I., Kessler, M., Weinstein, S., Franceschi, F. and Yonath, A. (2000) The identification of selected ribosomal components in crystallographic maps of prokaryotic ribosomal subunits at medium resolution. In The Ribosome: Structure, Function, Antibiotics and Cellular Interactions, R. Garrett, S. Douthwaite, A. Liljas, A. Matheson, P. Moore and H. Noller, eds. (Washington D.C., *ASM Press*), pp. 21-33.

von Böhlen, K., Makowski, I., Hansen, H.A.S., Bartels, H., Berkovitch-Yellin, Z., Zaytzev-Bashan, A., Meyer, S., Paulke, C., Franceschi, F. and Yonath, A. (1991). Characterization and Preliminary Attempts for Derivatization of Crystals of Large Ribosomal Subunits from Haloarcula marismortui, Diffracting to 3 Å Resolution. *J. Mol. Biol.* **222**, 1-15.

Brown, G.M., Noe-Spirlet, M.R., Busing W.R. and Levy, H.A. (1977). Dodecatungstophosphoric acid hexahydrate $(H_5O_2^+)_3(PW_{12}O_{40}^{-3})$. The true structure of Keggin's 'pentahydrate' from single-crystal X-ray and neutron diffraction data. *Acta Cryst.* **B33**, 1038-1046.

Cate, J.H. and Doubna, J.A. (1996). Metal binding sites in the major groove of a large ribozyme domain. *Structure* **4**, 1221-1229.

Cate, J.H., Yusupov, M.M., Yusupova, G.Z., Earnest, T.N. and Noller, H.F. (1999). X-ray crystal structure of 70S ribosome functional complexes, *Science* **285** 2095-2104.

Clemons, W. M., May, J.L.C., Wimberly, B.T., McCutcheon, J.P., Capel, M.S. and Ramakrishnan, V. (1999). Structure of a bacterial 30S ribosomal subunit at 5.5 Å resolution, *Nature* **400**, 833-840.

Contant, R., (1990). Potassium Octadecatungstodiphosphates(V) and Related Lacunary Compounds. *Inorg. Synth.* **27,** 104-111.

D'Amour, H., (1976). Comparison of the Heteropolyanions [PMo9O31(H2O)3]3-, [P2Mo18O62]6- and [P2W18O62]6-, *Acta Cryst***. B32**, 729-740.

Dawson, B. (1953). The structure of the 9(18)-heteropoly anion in potassium 9(18)-tungstophosphate, $K_6(P_2W_{18})O_{62})14H_2O$. *Acta Cryst*. **6**, 113-126.

Gabashivili, I.S., Agrawal, R.K., Grassucci, R. & Frank, J. (1999). Structure and structural variations of the E. coli 30S ribosomal subunit as revealed by three-dimensional cryo-electron microscopy. *J. Mol. Biol*. **286**,1285-1291.

Gewitz, H.S., Glotz, C., Piefke, J., Yonath, A. and Wittmann, H.G. (1988). Two-dimensional crystalline sheets of large ribosomal subunits containing nascent protein chain, *Biochimie* **70**, 645-651.

Golden, B.L., Gooding, A.R., Podell, E.R. and Cech, T.R. (1998). A preorgenized active site in the crystal structure of the tetrahymena ribozyme, *Science* **282**, 259-264.

Frank, J., Zhu, J., Penczek, P., Li, Y., Srivastava, S., Verschoor, A., Radermacher, M., Grassucci, R., Lata, A.R and Agrawal, R.K. (1995). A model of protein synthesis based on cryo electron microscopy of the *E. coli* ribosome. *Nature* **376**, 441-444.

Fu, J., Gnatt, A.L., Bushnell, D.A., Jansen, G.J., Thompson, N.E., Burges, R.R., David, P.R. and Korenberg, R.D. (1999). Yeast RNA Polymerase II at 5 Å resolution. *Cell* **98**, 799-810.

Harms, J., Tocilj, A., Levin, I., Agmon, I., Kölln, I., Stark, H., van Heel, M., Cuff, M., Schlünzen, F., Bashan, A., Franceschi, F. and Yonath, A. (1999). Elucidating the medium resolution structure of ribosomal particles: an interplay between electron-cryo-microscopy and X-ray crystallography. *Structure* **7**, 931-941.

Jahn, W. (1989). Synthesis of water soluble tetrairidium cluster for specific labelling of proteins. *Z. Naturforsch.* **44b**, 79-82.

Jones, T.A., Zou, J.-Y., Cowan, S.W. & Kjeldgaard, M. (1991). Improved methods for building protein models in electron density maps and the location of errors in these models. *Acta Cryst.* **A47**, 110-119.

Ladenstein, R., Bacher, A. and Huber, R. (1987). Some observations of a correlation between the symmetry of large heavy atom complexes and their binding sites on proteins. *J. Mol. Biol.* **195**, 751-3.

Liljas, A. and Al-Karadaghi, S. (1997). Structural aspects of protein synthesis. *Nature Structural Biology* **4**, 767-771.

Makowski, I., Frolow, F., Saper, M.A., Shoham, M., Wittmann, H.G. and Yonath, A. (1987). Single crystals of large ribosomal particles from Halobacterium marismortui diffract to 6 Å. *J. Mol. Biol.* **193**, 819-821.

Moore, P.B., Capel, M.S., Kjeldgaard, M. and Engelman, D.M. (1985). A 19 protein map of the 30S ribosomal subunit of E. coli. In "*Structure, Function & Genetics of Ribosomes"* (B. Hardesty & G. Kramer Eds.) Springer Verlag, Heidelberg & NY pp. 87-100.

Müller, F. and Brimacombe, R. (1997). A new model of the three-dimensional folding of *E. coli* 16S ribosomal RNA. II The RNA-protein interaction data. *J. Mol. Biol.* **271**, 524-544.

Nyborg, J., Nissen, P., Kjeldgaard. M., Thirup. S., Polekhina. G., Clark B.F.C. and Reshetnikova L. (1996). Structure of the ternary complex of EF-TU - macromoclecular mimicry in translation. *Trends in Biochemical Sciences* **21**, 81-82.

Pope, M.T. and Papaconstantinou, E., (1967). Heteropoly Blues. II. Reduction of 2:18-Tungstates, *Inorg. Chem.* **6**, 1147-1152.

Ramakrishnan, V. and White, S.W (1992). The structure of ribosomal protein S5 reveals sites of interaction with 16S RNA. *Nature* **358**, 768-771.

Ramakrishnan, V. & White, S.W (1998). Ribosomal protein structures: insights into the architecture, machinery and evolution of the ribosome, *Trends in Biochemical Sciences* **3**, 208-212.

Schlünzen, F., Kölln, I., Janell, D., Glühmann, M., Levin, I., Bashan, A., Harms, J., Bartels, H., Auerbach, T., Pioletti, T., Avila, H., Anagnostopoulos, K., Hansen, H.A.S., Bennett, W.S., Agmon, I., Kessler, M., Tocilj, A., Peretz, M., Weinstein, S., Franceschi, F. and Yonath, A. (1999). The identification of selected components in electron density maps of prokaryotic ribosomes at 7 Å resolution. *J. Syn. Radiation* **6**, 928-941.

Schlünzen, F., Tocilj, A., Zarivach, R., Harms, J., Glühmann, M., Janell, D., Bashan, A., Bartels, H., Agmon, I., Franceschi, F. and Yonath, A. (2000). Structure of a functionally activated small ribosomal subunit at 3.3 Å resolution. *Cell*, in press.

Stark, H., Müller, F., Orlova, E.V., Schatz, M., Dube, P., Erdemir, T., Zemlin, F., Brimacombe, R. and van Heel, M. (1995). The 70S *E. coli* ribosome at 23 Å resolution: fitting the ribosomal RNA. *Structure* **3**, 815-821.

Stöffler, G. and Stöffler-Meilicke, M. (1986). Immuno electron microscopy on E. coli ribosomes. In "*Structure, Function and Genetics of Ribosomes*" (B.Hardesty and G.Kramer Eds.) Springer Verlag, Heidelberg and NY. pp.28-46.

Tocilj, A., Schlünzen, F., Janell, D., Glühmann, M., Hansen, H.A.S., Harms, J., Bashan, A., Bartels, H., Agmon, I., Franceschi F. and Yonath, A. (1999). The small ribosomal subunit from *Thermus thermophilus* at 4.5 Å resolution: pattern fittings and the identification of a functional site. *PNAS* **96**, 14252-14257.

Trakhanov, S.D., Yusupove, M.M., Shirokov, V.A., Garber, M.B., Mitscher, A. Ruff, M., Tierry, J.-C. and Moras, D.(1989). Preliminary X-ray investigation on 70S ribosome crystals. *J. Mol. Biol.* **209**, 327-334.

Thygesen, J., Weinstein, S., Franceschi, F. and Yonath, A. (1996). On the suitability of multi metal clusters for phasing in crystallography of large macromolecular assemblies. *Structure* **4**, 513-518.

Wei, X., Dickman, M.H. and Pope, M.T. (1997). New Routes for Multiple Derivatization of Polyoxometalates: Diacetato-dirhodium-11-tungstophosphate *Inorg. Chem.* **36**, 130-131.

Weinstein, S., Jahn, W., Glotz, C., Schlünzen, F., Levin, I., Janell, D., Harms, J., Kölln, I., Hansen, H.A.S., Glühmann, M., Bennett, W.S., Bartels, H., Bashan, A., Agmon, I., Kessler, M., Pioletti, M., Avila, H., Anagnostopoulos, K., Peretz, M., Auerbach, T., Franceschi, F. and Yonath, A. (1999). Metal compounds as tools for the construction and the interpretation of medium resolution maps of ribosomal particles. *J. Struct. Biol.* **127**, 141-151.

Weller, J. W., and Hill, W.E. (1992). Probing dynamic changes in rRNA conformation in the 30S subunit of the E. coli Ribosome. *Biochemistry* **31**, 2748-2757.

Xin, F. and Pope, M.T. (1994). Polyoxometalate derivatives with multiple organic groups. 1. Synthesis and structure of tris(organotin) beta-keggin and alpha-Dawson tungstophosphates. *Organometallic*. **13**, 4881-4886.

Yonath, A. Glotz, C. Gewitz, H.S. Bartels, K. von Boehlen, K. Makowski, I. & Wittmann, H.G. (1988). Characterization of Crystals of Small Ribosomal Subunits, *J. Mol. Biol.* **203**, 831-833.

Yonath, A. Leonard K.R. and Wittmann, H.G. (1987). A tunnel in the large ribosomal subunit revealed by three dimensional image reconstruction *Science* **236**, 813-817.

Yonath, A. and Franceschi, F., (1998). Functional Universality and Evolutionary Diversity: Insights from the Structure of the Ribosome, *Structure* **6**, 678-684.

Yonath, A., Harms, J., Hansen, H.A.S., Bashan, A., Peretz, M., Bartels, H., Schlünzen, F., Kölln, I., Bennett, W.S., Levin, I., Krumbholz, S., Tocilj, A., Weinstein, S., Agmon, I., Piolleti, M., Janell, D., Auerbach, T. and Franceschi, F. (1998). The quest for the molecular structure of a large macromolecular assembly exhibiting severe non-isomorphism, extreme beam sensitivity and no internal symmetry. *Acta Cryst.* **54A**, 945-955.

Zamir, A., Miskin, R. and Elson, D. (1971). Inactivation and reactivation of ribosomal subunits: amino acyl-transfer RNA binding activity of the 30S subunit of *E. coli. J. Mol. Biol.* **60(2)**, 347-64.